ACCSCIENCE PUBLISHING

International Journal of Bioprinting

RESEARCH ARTICLE

Polydopamine-modified 3D-printed polycaprolactone scaffolds for promoting bone regeneration

Qian Zhong[1†], Shuai Huang[2†], Weihua Huang[2,3,4,5†], Hengpeng Wu[1], Yang Wang[2], Zhenyu Wen[1], Huinan Yin[2], Yixiao Wang[1], Weikang Xu[3,5*], and Qingde Wa[1*]

[1]Department of Orthopaedic Surgery, The Second Affiliated Hospital of ZunYi Medical University, Zunyi, Guizhou, China

[2]Department of Orthopaedic Surgery, The Second Affiliated Hospital of Guangzhou Medical University, Guangzhou, Guangdong, China

[3]Medical Materials and Engineering Research Laboratory, Institute of Biological and Medical Engineering, Guangdong Academy of Sciences, Guangzhou, Guangdong, China

[4]Department of Orthopaedic Surgery, The Affiliated Qingyuan Hospital (Qingyuan People's Hospital), Guangzhou Medical University, Qingyuan, Guangdong, China

[5]National Engineering Research Center for Healthcare Devices, Guangdong Key Lab of Medical Electronic Instruments and Polymer Material Products, Guangdong Institute of Medical Instruments, Guangdong Chinese Medicine Intelligent Diagnosis and Treatment Engineering Technology Research Center, Guangzhou, Guangdong, China

[†]These authors contributed equally to this work.

***Corresponding authors:**
Weikang Xu
(weikangxu1987@hotmail.com)

Qingde Wa
(wqd887zsy@126.com)

Citation: Zhong Q, Huang S, Huang W, et al. Polydopamine-modified 3D-printed polycaprolactone scaffolds for promoting bone regeneration. *Int J Bioprint*. 2025;11(1):418-438. doi: 10.36922/ijb.4995

Received: September 29, 2024
1st revised: November 6, 2024
2nd revised: December 16, 2024
Accepted: December 25, 2024
Published Online: December 26, 2024

Abstract

Polycaprolactone (PCL) is one of the most widely used three-dimensional (3D) printing materials with excellent biocompatibility and mechanical properties. However, its hydrophobic nature hinders cell adhesion and proliferation. Polydopamine (PDA) has been shown to promote proliferation and induce osteogenic differentiation of bone marrow mesenchymal stem cells (BMSCs) on polymer surfaces. Despite this, the impact of varying PDA coating thicknesses on the osteogenic differentiation of BMSCs has been minimally explored. In this paper, PCL scaffolds were fabricated using 3D printing technology, and PDA-coated PCL scaffolds (PDA-PCL-0, PDA-PCL-3, PDA-PCL-6, PDA-PCL-24) were prepared by immersing the scaffolds in an aqueous dopamine solution for fixed time points (0, 3, 6, 24 h) under constant shaking. The scaffolds were characterized and subjected to physicochemical performance tests to evaluate their effects on BMSC proliferation, adhesion, and osteogenic differentiation. The results showed that PDA-PCL-6 scaffolds exhibited significant immunomodulatory properties, promoting BMSC proliferation, adhesion, and osteogenic differentiation more effectively than the other groups. *In vivo* validation experiments, including micro-computed tomography, hematoxylin and eosin staining, Masson staining, and immunohistochemical analysis of bone morphologenetic protein 2 (BMP-2) and type I collagen (COL-I), confirmed that PDA-PCL-6 scaffolds significantly enhanced bone regeneration, histocompatibility, and hemocompatibility compared to uncoated scaffolds at 1, 2, and 3 months postoperation. In conclusion, our results indicate that a PDA coating obtained through 6-h immersion significantly enhances the biocompatibility and osteoinductive properties of PCL scaffolds, providing a promising strategy for bone defect repair.

Keywords: 3D printing; Bone regeneration; Polycaprolactone; Polydopamine

1. Introduction

The repair of bone defects resulting from trauma, infection, tumors, surgery, or other causes remains a significant challenge for orthopedic and plastic surgeons.[1] Bone defects larger than the critical size are beyond the organism's natural reparative capacity and require the intervention of bone graft substitutes.[2] Currently, autologous and allogeneic bone grafts are considered the gold standard for treating bone defects. However, their use is limited by disadvantages such as donor site hemorrhage, infection, pain, and the restricted availability of graft material.[3,4] Fortunately, in recent years, the rapid development of bone tissue engineering has led to the emergence of a wide variety of bone substitutes, offering promising materials for bone defect repair. Among these, 3D printing technology plays an important role in fabricating bone tissue engineering scaffolds. Its ability to control shape, structure, and porosity enables anatomical matching of bone defects, making it a valuable tool in bone defect treatment.[5]

Polycaprolactone (PCL), a hydrophobic aliphatic polyester, has been widely studied in biomedical applications due to its excellent biocompatibility, mechanical properties, low melting point (60 °C), and ease of processing.[6,7] However, PCL's hydrophobic nature, attributed to the multiple $-CH_2$ groups in its molecular structure, presents challenges for cell adhesion. This limitation hampers the attachment and growth of osteoblasts and neovascularization, both of which are critical for effective bone repair and regeneration. To address this issue, surface modification techniques have been proposed to augment the bioactivity of PCLscaffolds.[8] For example, Gharibshahian et al.[9] demonstrated that incorporating ceramic materials such as beta-tricalcium phosphate and hydroxyapatite, as well as magnesium oxide, improved the hydrophilicity, surface roughness, degradation rate, and osteoinductive properties of PCL scaffolds. Kikionis et al.[10] reported that PCL scaffolds combined with chlorella sulfated polysaccharide using a freeze-drying method promoted human bone marrow mesenchymal stem cell (BMSC) adhesion and osteogenic differentiation. Similarly, Wang et al.[11] showed that surface modification of PCL scaffolds with ZIF-8 and ZIF-8-mediated hydroxyapatite deposition increased surface roughness and significantly enhanced their *in vitro* and *in vivo* osteoinductivity and biocompatibility. Despite these promising results, the preparation processes for these surface-modified materials are often cumbersome.

Polydopamine (PDA) has emerged as a highly active coating material due to its molecular structure, which is rich in reactive functional groups such as –OH and $-NH_2$. These groups enable PDA to form strong bonds with the surfaces of various materials and cells, thereby facilitating cell–material adhesion and enhancing bioactivity. This interaction accelerates the healing of bone injuries.[12,13] By adjusting the reaction time between the PDA and the substrate material, the extent of surface functionalization can be meticulously controlled.[14]

Several studies have highlighted the osteogenic potential of PDA coatings. For instance, Teixeira et al.[15] demonstrated that PDA-coated polylactic acid scaffolds significantly enhanced alkaline phosphatase expression in mesenchymal stem cells, indicating improved bioactivity and osteogenic potential. Lin et al.[16] enhanced the hydrophilic and osteogenic properties of PCL scaffolds through PDA coating modification, though their study did not examine the effects of different PDA coating thicknesses or include *in vivo* data to support their findings. Xu et al.[17] observed that increasing PDA coating thickness promoted cell adhesion and proliferation, as well as improved osteogenesis. However, their study did not identify differences in the osteogenic effects of varying PDA coating thicknesses.

While these studies emphasize the excellent osteogenic properties of PDA coatings, they leave significant gaps in understanding the effects of different PDA coating thicknesses on immunomodulation and osteogenesis.

In this study, we prepared PCL scaffolds using a 3D printing technique with PCL as the raw material. The composite scaffold preparation process was designed to be simple and efficient by controlling the immersion time in dopamine aqueous solution to form PDA coatings of varying thicknesses on the scaffold surface. The performance of these PDA-coated scaffolds was then evaluated in terms of their ability to modulate macrophage polarization, promote cell proliferation and adhesion, enhance osteoinduction, and facilitate cranial bone defect repair.

2. Materials and methods

2.1. Materials

Polycaprolactone was purchased from Jinan Daigang Biotechnology Co. (China). Tris–HCl buffer (pH 8.5), dopamine hydrochloride (DA), $FeCl_3$, and $NH_3{\cdot}H_2O$ were obtained from McLean (XXX). Alkaline phosphatase assay kits and alizarin red staining kits were provided by Biyuntian Biotechnology Co (China). Ultrapure RNA kits, HiFi Script cDNA synthesis kits, and Ultra SYBR Mixture (Low ROX) were purchased from CWBIO (China). DMEM medium, fetal bovine serum, penicillin-streptomycin solution, phosphate buffer, trypsin, and CCK-8 kits were purchased from Gibco (China). Rat bone

marrow mesenchymal stem cells (BMSCs) were obtained from Shanghai Yansheng Industrial Co., Ltd. (China), and RAW264.7 cells was provided by Tongpai Biotechnology Co., Ltd. (China).

2.2. Preparation of polydopamine-polycaprolactone scaffolds

2.2.1. Printing of scaffolds

The scaffold model was designed using SolidWorks software, saved in STL format, and prepared for printing PCL. PCL particles were dried in a drying oven at 40 °C for 24 h and then added to the cartridge of a 3D printer (EFL-BP-6603, Suzhou Intelligent Manufacturing Research Institute, China). The preset model was loaded into the 3D printer system control software on the computer console, and the printing parameters were set as follows: needle inner diameter, 0.35 mm; holder diameter, 5 mm; aperture diameter, 300 μm; filament diameter, 350 μm; scaffold shape, porous cylinder; printing temperature, 60 °C; printing air pressure, 300 kPa; and printing speed, 10 mm/s. The printhead was activated to create the specified 3D porous cylindrical scaffolds. Scaffolds with a diameter of 10 mm and a height of 5 mm were reserved for mechanical strength tests, while the scaffolds with a diameter of 5 mm and a height of 1 mm were used for performance and cell experiments.

2.2.2. Polydopamine coating preparation

To prepare the DA solution, 50 mg of DA was dissolved in Tris–HCl buffer and stirred thoroughly to achieve a concentration of 2.5 mg/mL. The PCL scaffolds were immersed in the prepared DA solution and placed on a shaker for 0, 3, 6, and 24 h. After shaking, the samples were rinsed with deionized water to remove the unattached PDA and vacuum-dried for 24 h. The samples were categorized into four groups based on the immersion time as follows: PCL (control, also referred to as PDA-PCL-0), PDA-PCL-3, PDA-PCL-6, and PDA-PCL-24.

2.3. Physical and chemical properties of the scaffolds

2.3.1. Surface morphology and elemental composition of the scaffolds

Four groups of scaffolds were attached to the operating table using conductive adhesive, and their surfaces were sputter-coated with gold. The microscopic morphology and structure of the scaffolds were observed using a scanning electron microscope (SEM) (Phenom Prox, Merlin, the Netherlands) at an accelerating voltage of 10 kV. Our elemental analysis of the scaffolding was done using SEM (Phenom Prox, the Netherlands).

2.3.2. Fourier-transform infrared spectroscopy analysis

Scaffolds from each group were placed on the operating table of the Fourier-transform infrared (FTIR) spectrometer (Nicolet iS10, Thermo fisher, USA). The characteristic infrared absorption peaks of the scaffolds were analyzed in iso-ATR mode over a wave number range of 4000–400 cm^{-1}.

2.3.3. Porosity detection of the scaffolds

The porosity of the scaffolds was determined using a specific gravity flask 10ml (Shanghai Lugu Instrument Co., Ltd. China) method. The following measurements were recorded:

- M_0: The mass of the dried scaffold sample.
- M_1: The total mass of a specific gravity flask filled with anhydrous ethanol at room temperature.
- M_2: The total mass of the flask after placing the scaffold sample inside and ultrasonically treating it for 10 min to remove air bubbles.
- M_3: The residual mass of the scaffold after it was removed and weighed.

The porosity (P) was calculated using **Equation I**:

$$P = (M_2 - M_3 - M_0)/(M_1 - M_3) \quad \text{(I)}$$

2.3.4. Mechanical strength test of the scaffolds

The compressive modulus of the scaffolds was measured using a universal mechanical testing machine (345C-S, Instron, United States of America). At room temperature, the height of the scaffold was measured using a vernier caliper, and the scaffold was then placed on the test platform. The extrusion speed was set at 5 mm/min, and the test was terminated when the scaffold reached 80% compression deformation. During the compression plateau period, the pressure value was recorded as the compressive strength of the scaffold.

2.3.5. Dopamine release performance

Two steps were performed to assess dopamine release performance. These were following:

2.3.5.1. Step 1: Plotting the standard curve for DA release

A series of DA solutions with different concentration gradients (0, 1, 2.5, 5, 10, 15, 20, 25, and 50 μg/mL) were prepared. Into a 25 mL volumetric flask, 0.8 mL of $FeCl_3$ (1.992×10^{-2} mol/L) was pipetted, followed sequentially by 0.5 mL of DA solution and 0.5 mL of $NH_3{\cdot}H_2O$ (0.5 mol/L). The solution was diluted to the mark with water. Under alkaline conditions, $FeCl_3$ reacted with DA to

form a purplish-red compound. The absorbance was measured at 507 nm using an enzyme meter (United States of America), and a standard curve of DA concentration versus absorbance was generated.

2.3.5.2. Step 2: DA release testing

The scaffolds were placed in 48-well plates, and 1 mL of water was added to each well. The soaking solutions were collected on days 1, 3, 5, 7, and 14. The absorbance of each solution was measured using the method described above, and the DA release performance of each scaffold group was calculated based on the standard curve.

2.4. Cellular experiments

2.4.1. Cell culture and scaffold sterilization

Bone marrow-derived mesenchymal stem cells and RAW264.7 cells were cultured after resuscitation in a thermostatic cell culture incubator (MCO-18AIC, PHCbi, Japan) at 37 °C with 5% CO_2. The complete culture medium consisted of a high-glucose DMEM medium supplemented with 10% fetal bovine serum, 100 μg/mL penicillin, and 100 μg/mL streptomycin. The medium was replaced daily or every 2 days, depending on the cell condition. Cells were passaged upon reaching 70–80% confluence, and only cells at passages 3–5 were used for further experiments.

Scaffolds in each group were sterilized by soaking in 75% ethanol for 2 h, followed by three rinses with phosphate-buffered saline. The scaffolds were then placed overnight in a UV sterilizer (30–800 L, Shengzhiyuanhe Scientific and Educational Equipment Co., Ltd., China).

2.4.2. Cell adhesion evaluation

Bone marrow-derived mesenchymal stem cells from the third passage in the logarithmic growth phase were used. A cell suspension was prepared by digesting the cells with trypsin and resuspending them in a growth medium. The cells were seeded onto the surfaces of four groups of scaffolds at a density of 1×10^5 cells/cm^2 and cultivated in 48-well plates for 24 h.

After incubation, the culture medium was removed, and the scaffolds were transferred to new well plates using sterilized forceps. The cells on the scaffold surfaces were fixed with 2.5% glutaraldehyde buffer. The scaffolds were dehydrated using a graded ethanol series (30%, 50%, 70%, 80%, 90%, 95%) for 15 min at each concentration, followed by 20 min in anhydrous ethanol. The samples were air-dried naturally.

After dehydration, the scaffolds were mounted onto specimen holders and sputter-coated with gold. The surface morphology of the scaffolds after cell seeding, as well as the morphology and distribution of the BMSCs, was observed using SEM.

2.4.3. Cell proliferation evaluation

Bone marrow mesenchymal stem cells from the third passage, harvested during the logarithmic growth phase, were used in this study. A cell suspension was prepared by digesting the cells with trypsin and resuspending them in a growth medium. BMSCs were seeded onto the surfaces of the scaffolds at a density of 1×10^5 cells/cm^2 and cultured in 48-well plates. Following incubation for 1, 3, and 7 days, the medium was removed, and the scaffolds were transferred into new 48-well plates using forceps. Subsequently, a 10% cell counting Kit-8 (CCK-8) solution was added to each well, and the plate was incubated at 37 °C in a 5% CO_2 environment for 2 h. The absorbance at 450 nm was measured using a microplate reader to assess the proliferative capacity of the cells on the scaffolds.

2.4.4. Evaluation of macrophage polarization and osteogenic differentiation induced by the scaffolds

RAW264.7 macrophage cells were seeded onto the scaffolds in 48-well plates at a density of 5×10^4 cells per well. The complete medium was replaced every 2–3 days. On day 3, the expression levels of the M1 polarization marker geneinterleukin-1 beta (*Il1b*) and the M2 polarization marker gene *Cd206* were analyzed in the macrophage cells using polymerase chain reaction (PCR). Glyceraldehyde phosphate dehydrogenase (*Gapdh*) was used as the internal reference gene.

Bone marrow mesenchymal stem cells (1×10^5 cells per well) were seeded onto 48-well plates containing the scaffold samples. The osteogenic induction medium was prepared using a DMEM complete medium, supplemented with 0.39 mg dexamethasone, 1.76 mg vitamin C, and 306.11 mg sodium β-glycerophosphate per 100 mL. The BMSCs were cultured under osteogenic induction conditions for 14 days. At the end of the culture period, real-time fluorescence quantitative PCR (RT-PCR) was used to measure the expression of osteogenic marker genes, including alkaline phosphatase (*Alp*), Runt-related transcription factor 2 (*Runx2*), and collagen type I (*Col1*). *Gapdh* was used as the internal reference gene, the primer sequences used for real-time quantitative polymerase chain reaction of selected gene transcripts including Cd206 and Il1b are shown in Table 1. The data were analyzed using the $2^{-\Delta\Delta Ct}$ method, calculated as follows:

$$\Delta\Delta Ct = (Ct_{\text{target gene}} - Ct_{Gapdh})^{\text{experimental group}} - (Ct_{\text{target gene}} - Ct_{Gapdh})^{\text{control group}} \quad \text{(II)}$$

The relative expression (fold change) of each gene in the experimental group relative to the control group was calculated as $2^{-\Delta\Delta Ct}$.

Table 1. Primer sequences used for real-time quantitative polymerase chain reaction of selected gene transcripts

Gene transcript	Forward primer sequence (5'–3')	Reverse primer sequence (5'–3')
Gapdh	GCCATGAGGTCCACCACCCT	AAGGTCATCCCAGAGCTG
Alp	GGAGATGGTATGGGCGTCTC	GGACCTGAGCGTTGGTGTTA
Runx2	TCGGAGAGGTACCAGATGGG	AGGTGAAACTCTTGCCTCGT
Col1	TTCTCCTGGCAAAGACGGAC	CTCAAGGTCACGGTCACGAA
Cd206	ATGGATGTTGATGGCTACTGG	TTCTGACTCTGGACACTTGC
Il1b	TACAGGCTCCGAGATGAACA	AGGCCACAGGTATTTTGTCG

Alkaline phosphatase activity and calcium deposition were also evaluated to assess osteogenic differentiation. On day 7 of osteogenic induction, scaffolds were stained with an ALP staining kit. The bicinchoninic acid method was used for quantification of ALP enzyme activity. Briefly, cells in the well plates were lysed with lysis buffer according to the ALP assay kit instructions. The lysates were homogenized and centrifuged to extract the supernatant for the assay. The appropriate working solutions and samples were sequentially added to a 96-well plate. After incubation at 37°C for 30 min, the reaction was terminated, and absorbance was measured at 405 nm.

Calcium nodule staining and quantification of the scaffolds were performed on day 14 of osteogenic induction using the alizarin red staining kit. After staining, the scaffolds were photographed, and the alizarin red dye was extracted from the scaffolds using 10% cetylpyridinium chloride. The absorbance was measured at 562 nm to quantify calcium deposition.

2.5. *In vivo* evaluation of bone regeneration effect using a rat model for calvarial defects

A total of 27 male Sprague-Dawley (SD) rats, aged 8 weeks, were obtained from Zunyi Medical University (Guizhou, China) and housed in strict accordance with the recommendations in the Guide for Care and Use of Laboratory Animals of the National Institution of Health.

The rats were randomly assigned to three experimental groups of equal size (n = 9). Anesthesia was induced via intraperitoneal injection of a mixture containing 10% chloral hydrate and 25% urethane. Once anesthetized, the rats' scalps were shaved, and they were placed in a prone position on the operating table. The surgical site was disinfected with 1% iodine tincture and covered with a sterile drape. A midline incision (~2 cm) was made along the calvarium using a scalpel. Subcutaneous tissues were dissected using the blunt handle of the scalpel. The periosteum was gently incised along the sagittal suture of the skull, exposing the bilateral parietal bones, portions of the frontal bone, and portions of the occipital bone.

A 5-mm diameter full-thickness critical-sized bone defect was created bilaterally on the calvarium using a hollow trephine drill. The trephine bit was maintained perpendicular to the skull and operated at a low speed (1400–1500 rpm). As the drilling depth approached breakthrough, the applied force was reduced. At this point, relying solely on the weight of the trephine, the bit was tilted 20°–30° in the forward, backward, left, and right directions to gently complete the drilling. When only a small amount of bone remained connected, indicating that the drilling was almost complete, the looseness of the defect was tested with ophthalmic forceps, and the remaining bone around the circular defect was removed.

After the defect was created, the surgical site was rinsed with sterile saline. The bone defects were treated as follows (Figure 1): Group I received no scaffold (blank group), Group II received a PCL scaffold (control group), and Group III received a PDA-PCL scaffold (experimental group). Post-surgery, the rats were returned to their housing conditions, and penicillin (800,000 U/day) were administered intramuscularly for 3 consecutive days. The rats were sacrificed 4, 8, and 12 weeks post-implantation, after which the implants were dissected and prepared for micro-computed tomography (micro-CT) analysis and histological examination.

The histocompatibility test was performed by taking major organs such as heart, liver, spleen, lungs, and kidneys of rats and staining them with H&E sections.

2.6. Statistical analysis

Experimental data were expressed as mean ± standard deviation. Comparisons between groups were performed using one-way ANOVA in GraphPad Prism software. A p-value <0.05 indicated statistically significant differences, whereas p-values >0.05 indicated no significant differences between groups.

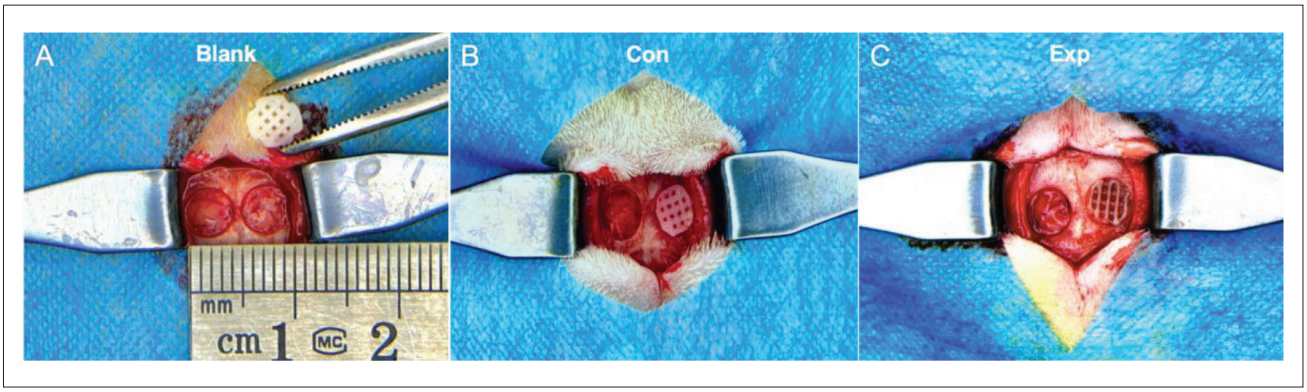

Figure 1. A rat cranial critical-sized defect of 5 mm was created. (A) Blank group (no scaffold). (B) Control group (pure PCL scaffold). (C) Experimental group (PDA-PCL scaffold).

3. Results

3.1. Characterization and physicochemical properties of scaffolds

The surface morphology of the four groups of scaffolds was observed using SEM at magnifications of 200×, 1000×, and 2000× (Figure 2A). The SEM analysis revealed that the fiber orientation of adjacent layers differed by 90°, with uniform coarseness and fineness. The scaffold surfaces exhibited a uniform pore distribution. In the PDA-modified groups (PDA-PCL-3, PDA-PCL-6, and PDA-PCL-24), grayish-black particles were observed on the scaffold surfaces. These particles resulted from the oxidative polymerization of DA on the surface of PCL, forming a PDA coating. The thickness of this coating increased with prolonged immersion times.[18]

Energy-dispersive X-ray spectroscopy analysis (Table 2) confirmed that no nitrogen atoms were detected in the PCL scaffolds. In contrast, nitrogen content increased in the PDA-modified scaffolds, measuring 5.99% in PDA-PCL-3, 6.82% in PDA-PCL-6, and 9.65% in PDA-PCL-24. This nitrogen content was attributed to the ethylamino group of PDA. Notably, the oxygen content rose to 32.11% in PDA-PCL-24 from 30.57% in the PCL group. In contrast, carbon and oxygen levels in the other PDA-coated scaffolds decreased compared to the PCL group. These variations likely resulted from the predominant contribution of the PCL substrate to the elemental composition and the limited depth of the energy spectral sweep.

Table 2. Elemental composition analysis of scaffolds of varying immersion duration in dopamine

Samples	Carbon (%)	Oxygen (%)	Nitrogen (%)
PCL	69.43	30.57	0
PDA-PCL-3	67.70	26.31	5.99
PDA-PCL-6	66.82	26.36	6.82
PDA-PCL-24	58.24	32.11	9.65

Further analysis revealed a gradual decrease in carbon content and a corresponding increase in oxygen content in the PDA-PCL-3, PDA-PCL-6, and PDA-PCL-24 groups with increasing immersion times. This trend aligned with the expected progression of DA oxidative polymerization. FTIR spectroscopy further confirmed the presence of PDA-specific reactive groups in the modified scaffolds. Peaks corresponding to O–H and N–H stretching vibrations were observed at 3000–3500 cm^{-1} (Figure 2B), with their intensity increasing with longer immersion times.

In the DA release experiments, based on the standard curve (Figure 2D), the PDA-PCL-24 scaffolds released approximately 40–72 nM of DA, PDA-PCL-6 released 33–44 nM, and PDA-PCL-3 released 5–7 nM (Figure 2E). Mechanical testing revealed that all scaffold groups exhibited a compressive strength of approximately 8 MPa (Figure 2C). Additionally, the porosity of all scaffolds was consistently around 75%, with no significant differences between groups. These findings indicate that the PDA coating did not change the original mechanical properties or porosity of the PCL scaffolds.

3.2. Effects of scaffolds on morphology and attachment of bone marrow mesenchymal stem cells

The extent of cell proliferation and adhesion to scaffolds is a critical factor in bone repair. To evaluate these parameters, we assessed the proliferative activity of BMSCs co-cultured with scaffolds using the CCK-8 assay on days 1, 3, and 7.

As shown in Figure 3B, the proliferative activity of cells on scaffolds with a PDA coating was significantly higher than that of the PCL group on days 1 and 3. By day 7, the

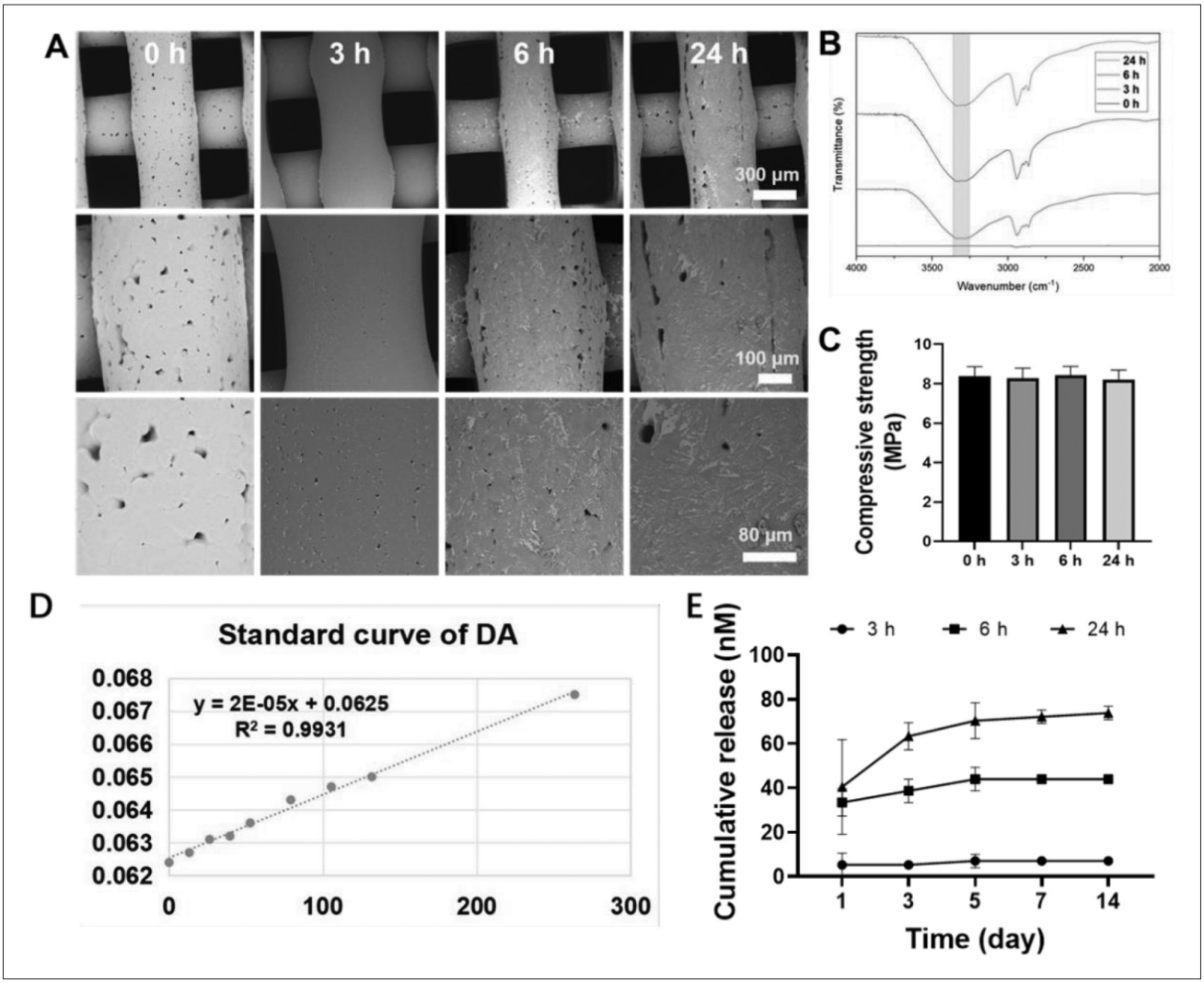

Figure 2. Material characterization and physicochemical property diagrams of the four groups of scaffolds. (A) Surface morphology. Scale bars: Top row: 300 μm; Middle row: 100 μm; Bottom row: 80 μm. Magnification: Top row: 200×; Middle row: 1000×; Bottom row: 2000×. (B) Fourier-transform infrared spectra. (C) Compression properties. (D) Standard curves for dopamine (DA) release. (E) DA release performance for each group. Notes: 0 h: The PCL group; 3 h: The PDA-PCL-3 group; 6 h: The PDA-PCL-6 group; 24 h: The PDA-PCL-24 group.

scaffolds in the PDA-PCL-6 group exhibited significantly enhanced pro-proliferative activity for BMSCs compared to the PCL group, whereas no significant differences were observed among the other groups.

Figure 3A displays SEM images of BMSCs adhering to the scaffolds after 1 day of culture. Numerous columnar and lamellar BMSCs were observed on the scaffold surfaces, with clear pseudopodia extending from the cells. These results were consistent with the cell proliferation findings. The PDA coating appeared to promote cell adhesion, with the PDA-PCL-6 group showing the most pronounced effect. In contrast, no significant differences in adhesion were noted between the PDA-PCL-3 and PDA-PCL-24 groups.

3.3. Evaluation of *in vitro* osteogenic and immunomodulatory properties of the scaffolds

To investigate the effects of PDA-coated scaffolds on the osteogenic differentiation of BMSCs, scaffolds were co-cultured with BMSCs. RT-PCR was used to analyze the expression of osteogenic genes, while ALP secretion and calcium nodule deposition were also evaluated.

As shown in Figure 4A and B, scaffolds with PDA coatings, particularly PDA-PCL-6, significantly enhanced ALP secretion compared to the other groups. Staining

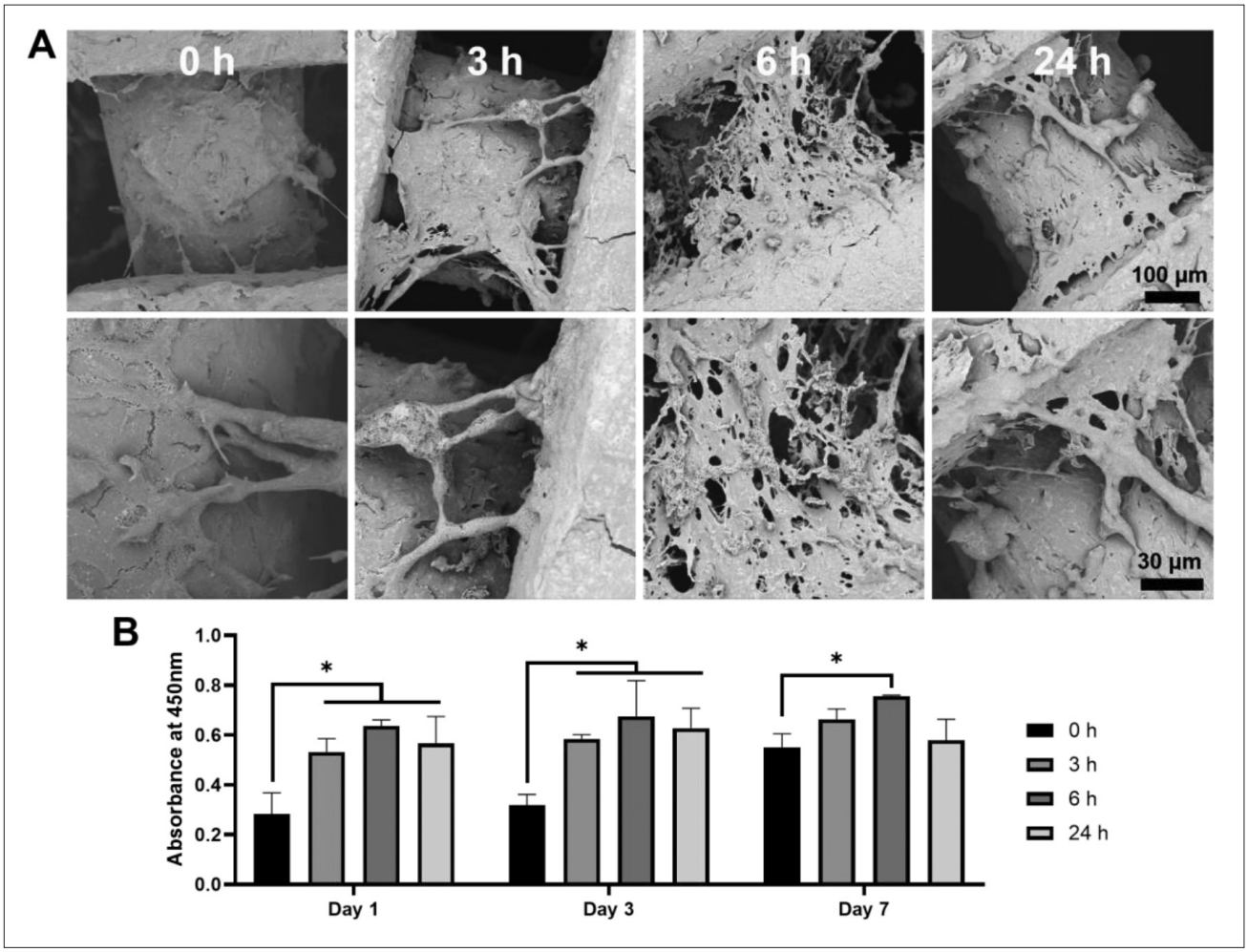

Figure 3. Enhanced bone marrow mesenchymal stem cell (BMSC) adhesion and proliferation on polydopamine-coated polycaprolactone scaffolds. (A) Scanning electron microscopic images showing BMSCs adhering to scaffolds after 24 h of culture. Scale bars: Top row: 100 μm; Bottom row: 30 μm. Magnification: Top row: 500×; Bottom row: 2000×. (B) Proliferation of BMSCs cultured on the four scaffold groups on days 1, 3, and 7. Notes: 0 h: The PCL group; 3 h: The PDA-PCL-3 group; 6 h: The PDA-PCL-6 group; 24 h: The PDA-PCL-24 group. *$p < 0.05$ indicates a significant difference against the PCL group.

and quantitative analysis of calcium nodules further demonstrated the superior performance of PDA-coated scaffolds. The PDA-PCL-6 group exhibited the highest calcium nodule content, while no significant differences were observed between the PDA-PCL-3 and PDA-PCL-24 groups (Figure 4C and D). These findings were in line with the trends observed in ALP secretion.

In terms of osteogenesis-related gene expression (*Runx2*, *Alp*, *Col1*) (Figure 4E), the PDA coating generally enhanced *Runx2* expression. The PDA-PCL-6 and PDA-PCL-24 groups showed similar expression levels, both of which were significantly higher than those in the PDA-PCL-3 group. *Alp* gene expression mirrored the ALP quantification results, with a significant increase observed in the PDA-PCL-6 group, while no significant differences were noted between the PDA-PCL-24 group and other groups. In terms of Col1 expression, compared with other groups, the PDA-PCL-6 group showed the highest expression level, and the PCL-3 group showed a higher expression level than the PCL group. There was no significant difference between the PDA-PCL-24, the PCL, and PCL-3 groups.

For immunomodulatory performance, PDA-coated scaffolds significantly upregulated the expression of *Cd206* and downregulated the expression of *Il1b* (Figure S2, Supporting Information). Among all groups, the PDA-PCL-6 group demonstrated the most pronounced ability to promote macrophage polarization from the M1 to

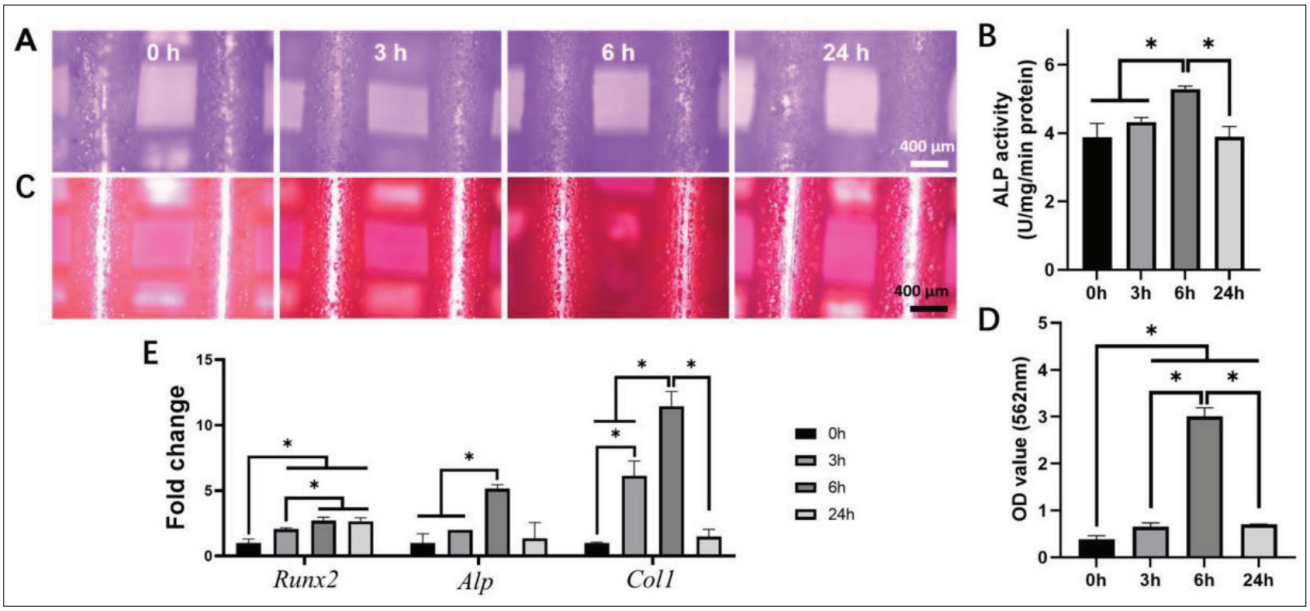

Figure 4. Evaluation of the enhanced *in vitro* osteogenic capacity of bone marrow mesenchymal stem cells (BMSCs) growing on the scaffolds. (A) Alkaline phosphatase (ALP) staining and (B) quantitative analysis of the scaffolds co-cultured with BMSCs on day 7. Scale bar: 400 μm. Magnification: 5×. (C) Calcium nodule staining and (D) quantitative plots of scaffolds co-cultured with BMSCs on day 14, respectively. Scale bars: 400 μm. Magnification: 5× (E) Expression of osteogenesis-related genes (*Runx2*, *Alp*, *Col1*) in BMSCs on day 14. Notes: 0 h: The PCL group; 3 h: The PDA-PCL-3 group; 6 h: The PDA-PCL-6 group; 24 h: The PDA-PCL-24 group. *$p < 0.05$ indicates a significant difference.

the M2 phenotype. This enhanced immunomodulatory performance is attributed to the oxidative free radical scavenging properties of PDA, which confer immunomodulatory activity to the scaffold, downregulate inflammatory cytokine expression, and stimulate the M2 macrophage phenotype.[19]

3.4. *In vivo* study of the scaffolds for bone regeneration

To evaluate the pro-regenerative properties of PDA-coated scaffolds *in vivo*, we selected PDA-PCL-6, which exhibited the highest bioactivity in the *in vitro* experiments, as the experimental group (Exp). A control group (Con; pure PCL) and a blank group (Blank) were also included. Micro-CT analysis was performed on the bone defect regions of three groups of SD rats at 4, 8, and 12 weeks postoperatively.

As depicted in Figure 5A, the blank group, which did not receive a scaffold implant, displayed minimal new bone formation within the defect area at both 4 and 8 weeks postoperatively. Even by 12 weeks, the increase in new bone tissue was negligible, suggesting a suboptimal bone repair process in the absence of a scaffold. In contrast, the PCL group, which was implanted with pure PCL scaffolds, showed some new bone formation at 4 weeks postoperatively. However, the increase in new bone tissue over the subsequent 8 and 12 weeks was insufficient to fully heal the substantial bone defect, highlighting the limited osteogenic potential of pure PCL scaffolds for bone repair.

The PDA-PCL group consistently demonstrated superior new bone formation compared to the PCL group at each time point. At 4 weeks, the growth of trabecular bone along the composite scaffold within the defect area was evident, and this growth progressively increased by 8 weeks. By 12 weeks, the defect area was nearly filled with trabecular and lamellar bone, indicating a significantly enhanced bone repair process.

Quantitative analysis of the bone volume fraction in the defect areas at 4, 8, and 12 weeks postoperatively, as presented in Figure 5B, confirmed that the PDA–PCL composite scaffolds provided superior bone repair efficacy. In comparison, the blank group exhibited the least favorable outcomes. Statistically significant differences were observed ($p < 0.05$), underscoring the enhanced osteoconductive properties of the PDA-modified scaffolds in promoting bone regeneration.

To further verify the *in vivo* bone defect repair effects of the three scaffold groups, rat skull specimens were collected at 4, 8, and 12 weeks postoperatively. Bone formation at the defect site was analyzed using hematoxylin and eosin (H&E) staining, Masson staining, and Movat staining.

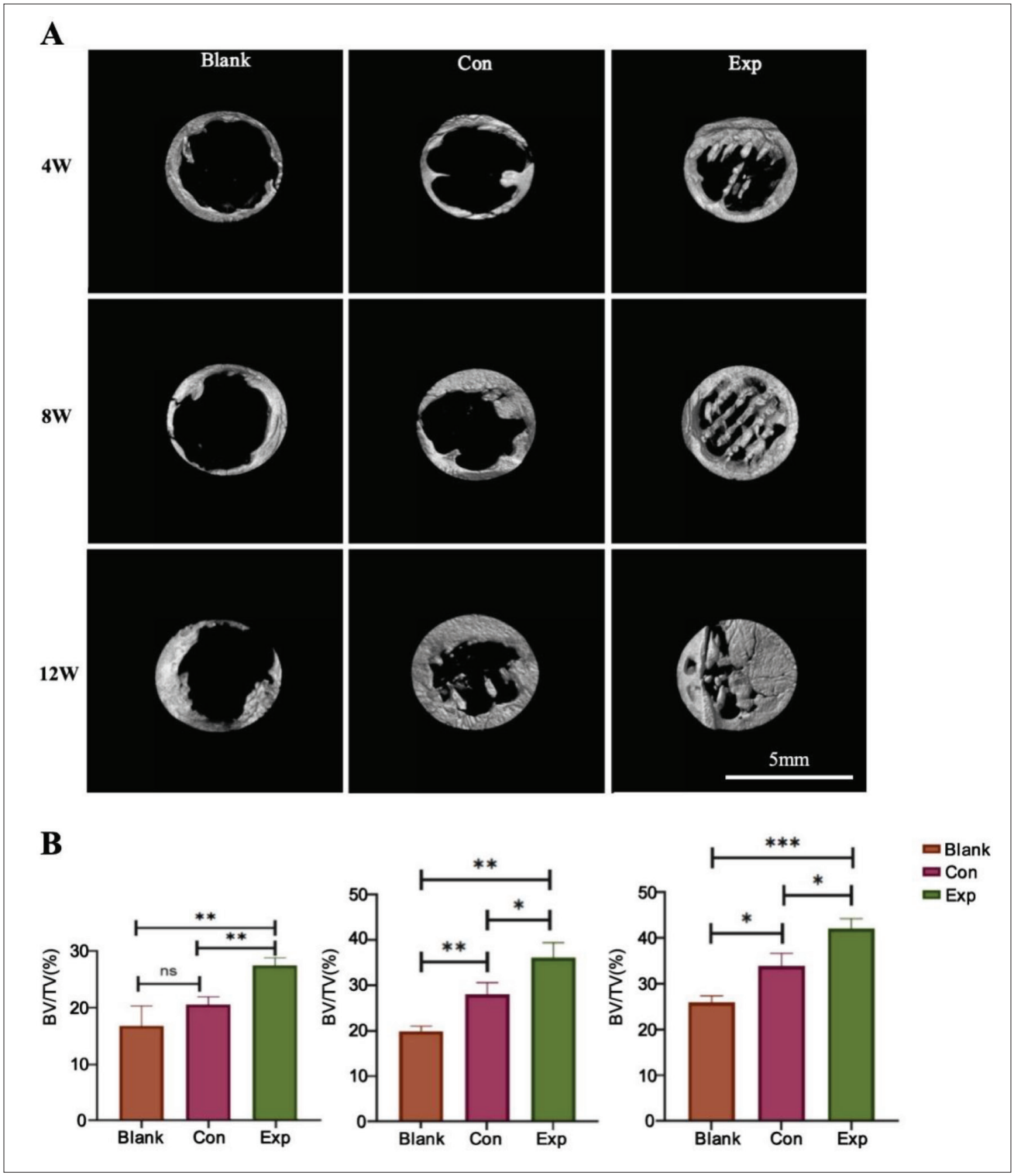

Figure 5. *In vivo* bone regeneration in a rat calvarial defect model. (A) Micro-computed tomography of rat calvarial defects at 4, 8, and 12 weeks postoperatively for each group. Scale bar: 5 mm. Magnification: 1.5×. (B) Quantitative analysis of bone volume fraction in the defect regions of rats at 4, 8, and 12 weeks (from left to right) for each group. Notes: Blank: No scaffold; Control: Treated with the PCL scaffold; Exp: Treated with the PDA-PCL scaffold. *$p < 0.05$ indicates a significant difference.

The H&E staining images at 4 weeks (Figure 6) revealed that the blank group exhibited a large amount of fibrous tissue and minimal new bone tissue in the bone defect area. In the PCL group, a small amount of new bone was observed within the defect area, whereas the PDA-PCL group showed significantly more new bone formation. At 8 weeks, the new bone tissue in the PDA-PCL group showed a wider distribution compared to the other two groups. Interconnected pores were filled with gradually forming new bone tissue, while osteoid tissue and small amounts of woven bone were observed at the material–bone interface and within the porous scaffold. By 12 weeks, as the PCL material degraded and the defect area further decreased, the new bone in the PDA-PCL group formed a continuous block. The new bone area in this group was significantly larger compared to the blank and PCL groups. Masson staining results (Figure 7) supported these findings. At 4 weeks, the PDA-PCL group showed more light blue collagen tissue and red muscle fiber tissue compared to the PCL group, with the least amount observed in the blank group. Over time, at 8 and 12 weeks, all groups exhibited further maturation of neoplastic bone tissue, with dark blue-stained mature collagen becoming prominent. This effect was most pronounced in the PDA-PCL group, followed by the PCL group.

Movat staining results (Figure 8) were in line with the trends observed in H&E and Masson staining. Movat staining identified collagen and reticulocyte fibers as yellow, proteoglycans as blue-green, and cellulose-like or fibrillar structures as dark red. In the PDA-PCL group, neoplastic bone tissue gradually replaced the scaffold, with a substantial presence of yellow-stained collagen fibers and reticular fibers forming more mature neoplastic bone and showing cortical bridging. In contrast, the blank group was dominated by muscle tissue with minimal neoplastic bone and insignificant cortical bridging. The PCL group demonstrated intermediate bone deposition and formation, falling between the other two groups.

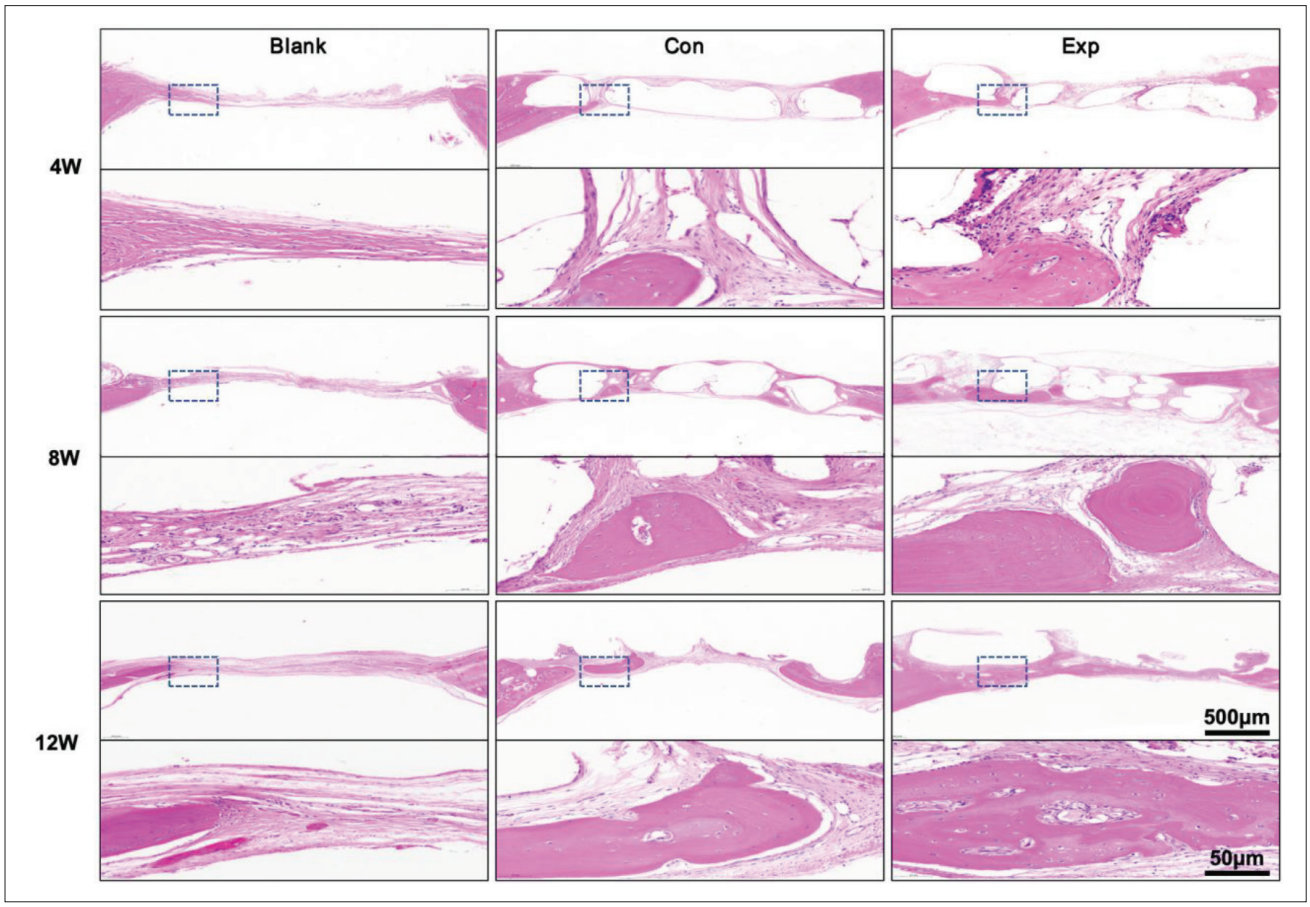

Figure 6. Hematoxylin and eosin staining of rat calvarial specimens at 4, 8, and 12 weeks postoperatively for each group. Scale bar: Top row of each time point: 500 μm; Bottom row of each time point: 50 μm. Magnification: Top row of each time point: 2×; Bottom row of each time point: 10×. Notes: Blank: No scaffold; Control: Treated with the PCL scaffold; Exp: Treated with the PDA-PCL scaffold.

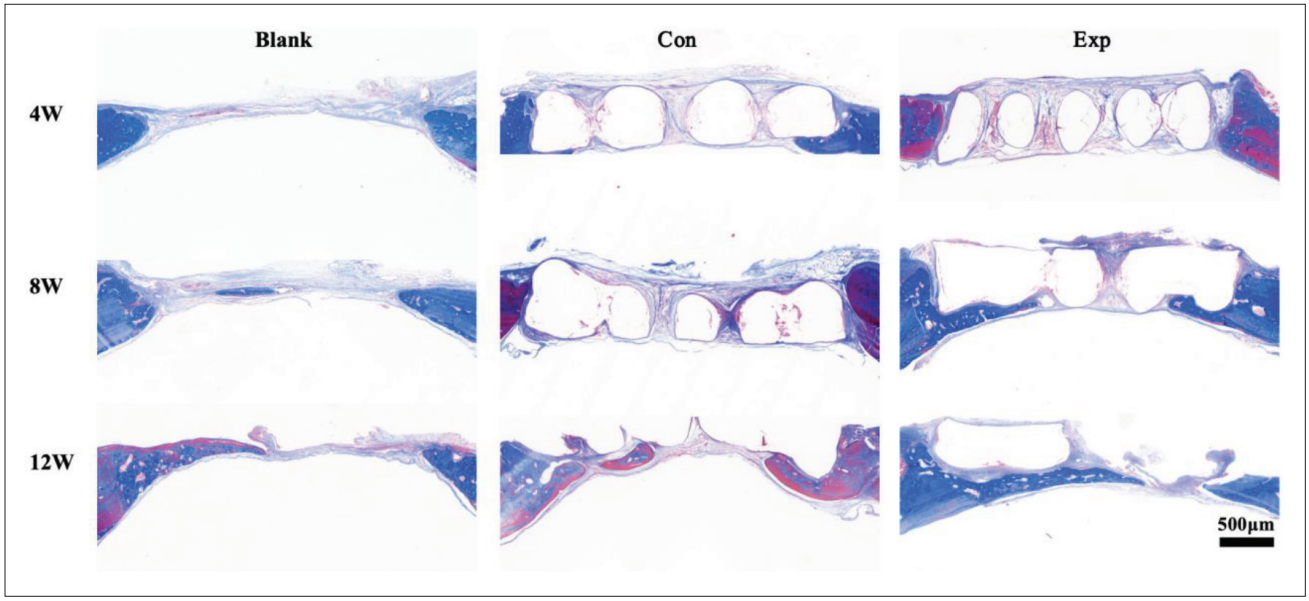

Figure 7. Masson staining of rat calvarial specimens at 4, 8, and 12 weeks postoperatively for each group. Scale bar: 500 μm. Magnification: 2×.

These results suggest that PDA-functionalized PCL scaffolds can effectively induce *in situ* bone regeneration without the need for exogenous seed cells or growth factors.

To further assess the osteoinductive potential of the scaffolds, immunohistochemical staining was performed to detect BMP-2 and COL-I expression in each group. As shown in Figures 9 and 10, at 4 weeks, distinct brown-yellow areas were observed around the newly formed tissue in the bone defect area of the PDA-PCL group, indicating positive expression of BMP-2 and COL-I. In contrast, the PCL group displayed only a few positive expression areas, while the blank group showed almost no detectable expression.

At 8 weeks, both the PDA-PCL and PCL groups showed discontinuous new bone formation. The PDA-PCL group exhibited deeper and more extensive brown-yellow positive expression areas around the new bone matrix for BMP-2 and COL-I, whereas the blank group showed only minimal BMP-2 and COL-I expression.

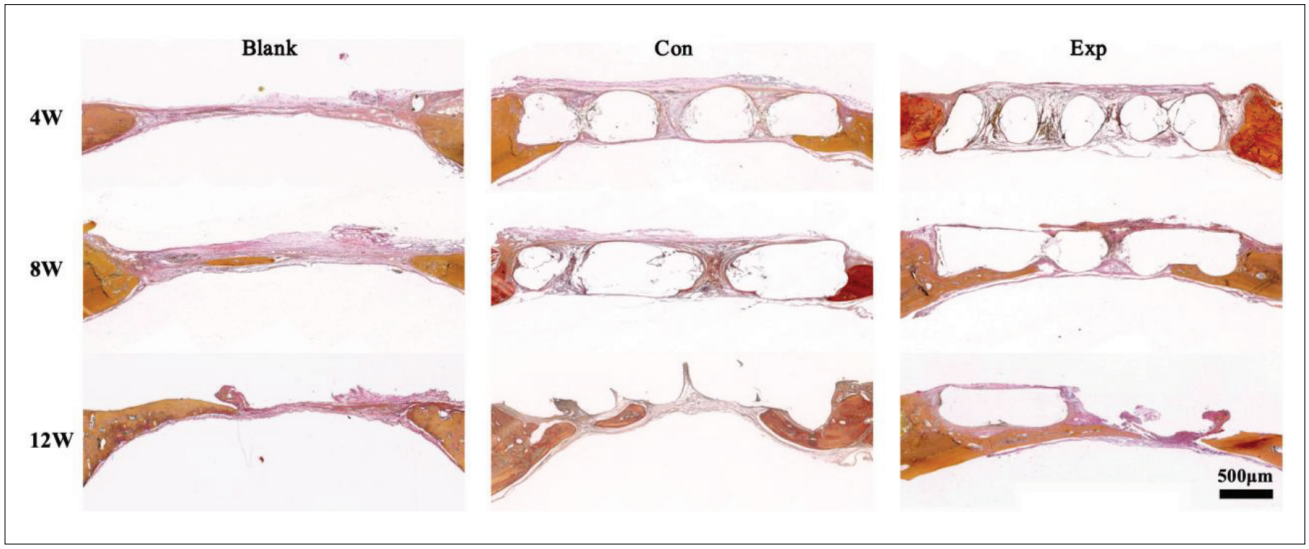

Figure 8. Movat staining of rat calvarial specimens at 4, 8, and 12 weeks postoperatively for each group. Scale bar: 500 μm. Magnification: 2×. Notes: Blank: No scaffold; Control: Treated with the PCL scaffold; Exp: Treated with the PDA-PCL scaffold.

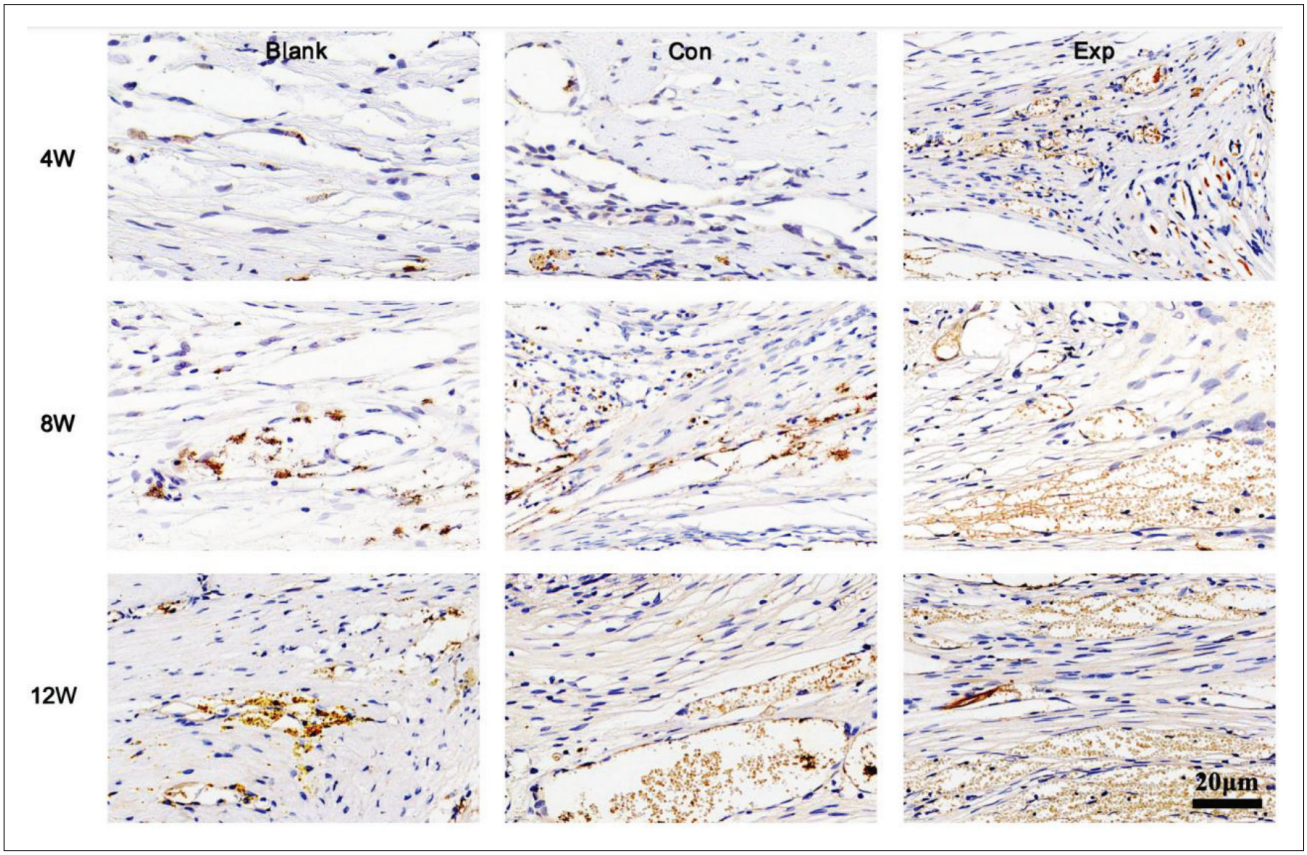

Figure 9. Immunohistochemical expression of BMP-2 in rat calvarial specimens at 4, 8, and 12 weeks postoperatively for each group. Scale bar: 20 μm. Magnification: 40×. Notes: Blank: No scaffold; Control: Treated with the PCL scaffold; Exp: Treated with the PDA-PCL scaffold.

By 12 weeks, BMP-2 and COL-I expression levels in the bone defect sites had increased across all groups compared to earlier time points. However, the PDA-PCL group demonstrated significantly greater positive expression than both the PCL and blank groups. These findings indicate that the PDA-functionalized coating significantly enhances the osteoinductive potential of PCL scaffolds and promotes the expression of bone tissue markers.

3.5. Histocompatibility of polydopamine-coated scaffolds *in vivo*

3.5.1. Blood indicator tests

The routine blood indices of rats from the three groups were measured at 4, 8, and 12 weeks postoperatively, as shown in Table 3. No statistically significant differences were observed among the blank group, PCL group, and PDA-PCL group in terms of white blood cell count, red blood cell count, hemoglobin, platelets, glutamate aminotransferase, glutamate aminotransferase, creatinine, and urea levels.

3.5.2. Hematoxylin and eosin staining of liver and kidney tissue

Liver and kidney specimens were collected from rats in each group, and histological sections were prepared and analyzed using H&E staining to identify pathological changes. As shown in Figure 11, liver structures such as the central vein, confluent areas, and hepatocytes were intact and well-defined across all groups, with normal size, morphology, and boundaries. No inflammatory cell infiltration was observed.

Similarly, kidney structures, including glomeruli, tubules, and mesangial cells, appeared normal in size, morphology, and boundaries across all groups, as shown in Figure 12. No signs of inflammatory cell infiltration were observed.

4. Discussion

Ideal bone repair materials should possess excellent biocompatibility, osteoinductivity, osteoconductivity, and osteointegration.[20] The biodegradable polymer

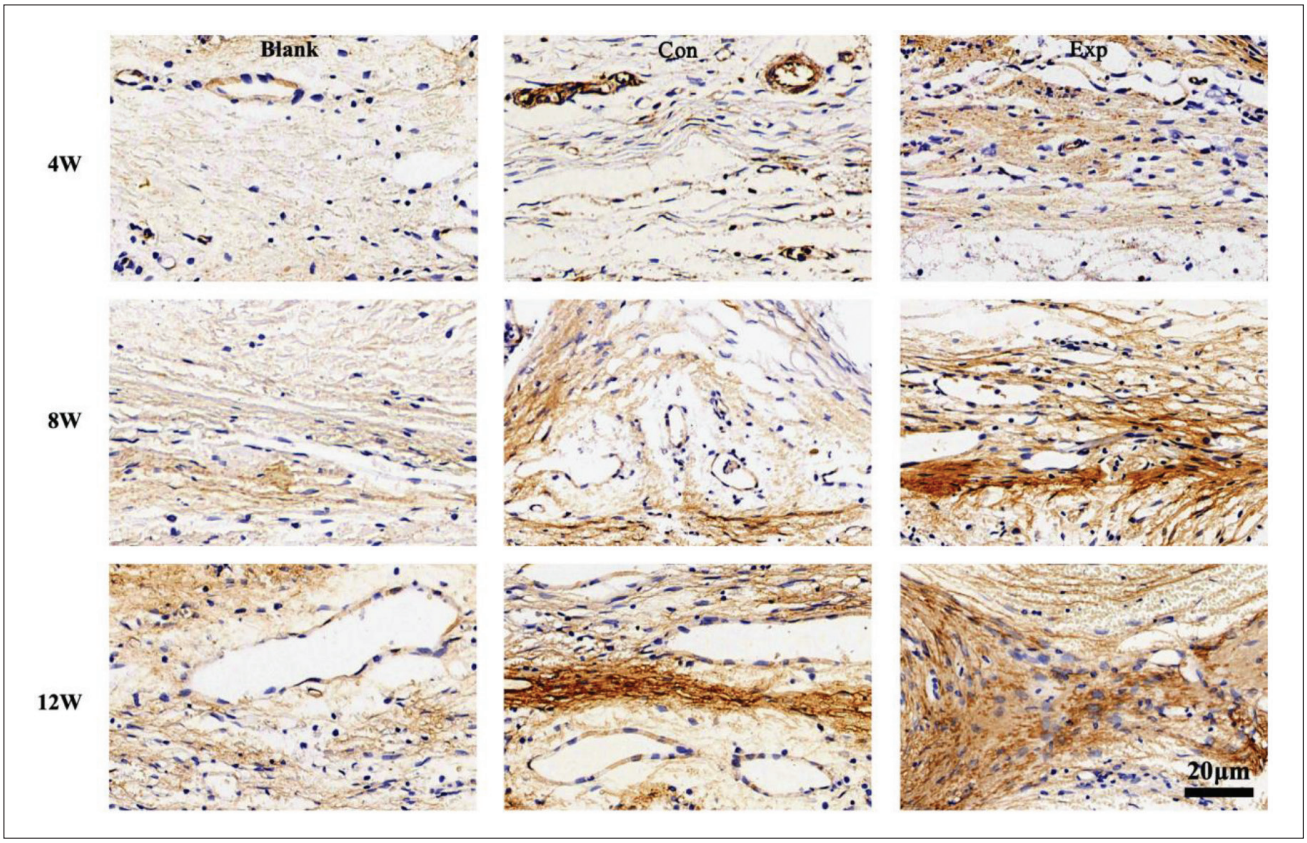

Figure 10. Immunohistochemical expression of COL-I in rat calvarial specimens at 4, 8, and 12 weeks postoperatively for each group. Scale bar: 20 μm. Magnification: 40×. Notes: Blank: No scaffold; Control: Treated with the PCL scaffold; Exp: Treated with the PDA-PCL scaffold.

PCL is widely used in bone tissue engineering due to its high plasticity and excellent biocompatibility. Upon degradation into water and carbon dioxide, PCL promotes bone defect repair while providing space for the ingrowth of new bone tissue and blood vessels, making it a suitable base material for bone tissue scaffolds.[21] However, PCL is inherently hydrophobic and lacks adequate sites for cell adhesion. Consequently, the single structure of PCL alone is insufficient to serve as an ideal bone scaffold material.[22]

Previous studies have shown that optimizing the 3D porous structure of scaffolds while maintaining mechanical strength and ensuring a highly interconnected internal pore network can significantly increase the surface area for cell attachment and enhance nutrient permeability.[23] For bone tissue engineering, scaffolds fabricated through 3D printing offer customizable geometric shapes and porosity, with micro-level interconnectivity that supports the ingrowth of bone tissue and blood vessels on the scaffold surface. These features facilitate nutrient delivery to cells and establish a strong connection with the host bone, showing good prospects for bone defect repair applications.[24] Previous research has shown that porous PCL scaffolds created using 3D printing significantly improved osteogenic effects in a pig condyle bone defect model.[25]

Numerous studies have highlighted the importance of surface characteristics and material–cell interactions in effective bone defect repair.[26] Functional modification of material surfaces can enhance hydrophilicity, adhesion, and interaction with cells and tissues, thereby improving biocompatibility.[27] PDA, a melanin-like substance, contains multiple active functional groups, such as catechol and hydrophilic amino groups. These groups enable PDA to strongly attach to material surfaces through covalent bonds, improving hydrophilicity, adhesion, and biocompatibility without eliciting an immune response in the human body.[28,29] Additionally, the catecholamine groups in PDA exhibit strong chelation with calcium ions, promoting calcium ion enrichment on scaffold surfaces and enhancing mineralization. This property further supports bone repair by increasing the scaffold's osteoinductive potential.[30]

In this study, 3D printing was used to fabricate PCL scaffolds, which were subsequently surface-modified with

Table 3. Blood indices of rats in each group at 4, 8, and 12 weeks postoperatively

Time point (week)	Clinical test indicators	Group			*p-value*
		Blank	Control	Experimental	
4	WBC (10^9/L)	11.15 ± 0.46	10.36 ± 0.86	11.68 ± 0.61	0.125
	RBC (10^{12}/L)	8.99 ± 0.61	8.12 ± 0.17	8.44 ± 0.58	0.655
	HB (g/L)	153.33 ± 4.73	162.00 ± 8.89	159.00 ± 7.81	0.399
	PLT (10^9 L)	936.67 ± 130.62	1005.00 ± 100.58	902.67 ± 140.76	0.619
	ALT (U/L)	53.00 ± 2.65	50.67 ± 3.06	53.33 ± 2.52	0.477
	AST (U/L)	113.67 ± 2.08	116.33 ± 4.16	118.33 ± 1.53	0.209
	Urea (mmol/L)	4.23 ± 0.15	4.83 ± 0.92	4.06 ± 0.27	0.281
	Cr (μmol/L)	37.33 ± 1.53	36.33 ± 5.69	31.33 ± 1.53	0.161
8	WBC (10^9/L)	9.89 ± 1.10	9.45 ± 1.35	9.44 ± 1.83	0.915
	RBC (10^{12}/L)	8.20 ± 0.28	8.74 ± 0.66	9.09 ± 0.84	0.304
	HB (g/L)	159.00 ± 8.72	157.67 ± 8.50	166.67 ± 6.03	0.378
	PLT (10^9/L)	897.33 ± 17.90	1000.00 ± 81.07	997.00 ± 207.65	0.572
	ALT (U/L)	41.67 ± 7.02	48.33 ± 3.79	45.00 ± 11.79	0.633
	AST (U/L)	122.00 ± 29.61	127.33 ± 22.03	134.67 ± 20.55	0.821
	Urea (mmol/L)	5.04 ± 0.68	4.73 ± 0.53	4.95 ± 0.23	0.764
	Cr (μmol/L)	36.67 ± 4.04	35.00 ± 3.61	34.33 ± 4.93	0.792
12	WBC (10^9/L)	10.49 ± 0.14	10.04 ± 0.23	10.27 ± 0.37	0.188
	RBC (10^{12}/L)	8.42 ± 0.40	8.90 ± 0.32	8.55 ± 0.38	0.315
	HB (g/L)	166.33 ± 3.79	168.00 ± 7.94	169.67 ± 3.51	0.766
	PLT (10^9/L)	945.33 ± 38.19	995.33 ± 25.42	991.33 ± 44.55	0.260
	ALT (U/L)	37.33 ± 3.79	35.00 ± 4.36	37.00 ± 1.73	0.690
	AST (U/L)	97.67 ± 5.03	96.67 ± 7.23	94.33 ± 4.16	0.767
	Urea (mmol/L)	4.96 ± 0.22	4.76 ± 0.43	4.76 ± 0.27	0.673
	Cr (μmol/L)	33.33 ± 3.06	36.33 ± 1.15	32.33 ± 2.52	0.182

Notes: Values are expressed as mean ± standard deviation. ALT, glutamate aminotransferase; AST, glutamate aminotransferase; Cr, creatinine; HB, hemoglobin; PLT, platelet; RBC, red blood cell count; WBC, white blood cell count.

PDA. The repair capacity of the PDA–PCL composite scaffolds was evaluated by comparing their physical properties, biocompatibility, *in vitro* osteoinductive potential on BMSCs, and *in vivo* osteoinductive potential on rat calvarial defect models. This approach provided a comprehensive assessment of the repair capabilities of PDA–PCL composite scaffolds in comparison to unmodified PCL scaffolds.

Polycaprolactone scaffolds were prepared using 3D printing technology, and PDA coating was applied via an immersion shaker method. The results (Figure 2) showed that the surface of the modified scaffolds became rougher due to the oxidative polymerization of DA, forming a PDA coating. PDA adheres to hydroxyl-containing PCL surfaces through chelation, hydrogen bonding, π-π stacking, and other non-covalent interactions.[31] This increased surface roughness significantly enhanced cell adhesion and proliferation.[32]

Elemental composition analysis and FTIR spectroscopy confirmed the presence of nitrogen on PDA-modified scaffolds, with nitrogen content and the characteristic PDA peak at 3000–3500 cm^{-1} increasing with immersion times. This increase was attributed to the introduction of surface amine groups from the PDA attachment, confirming the successful preparation of PDA-PCL scaffolds.[33] Although the compressive

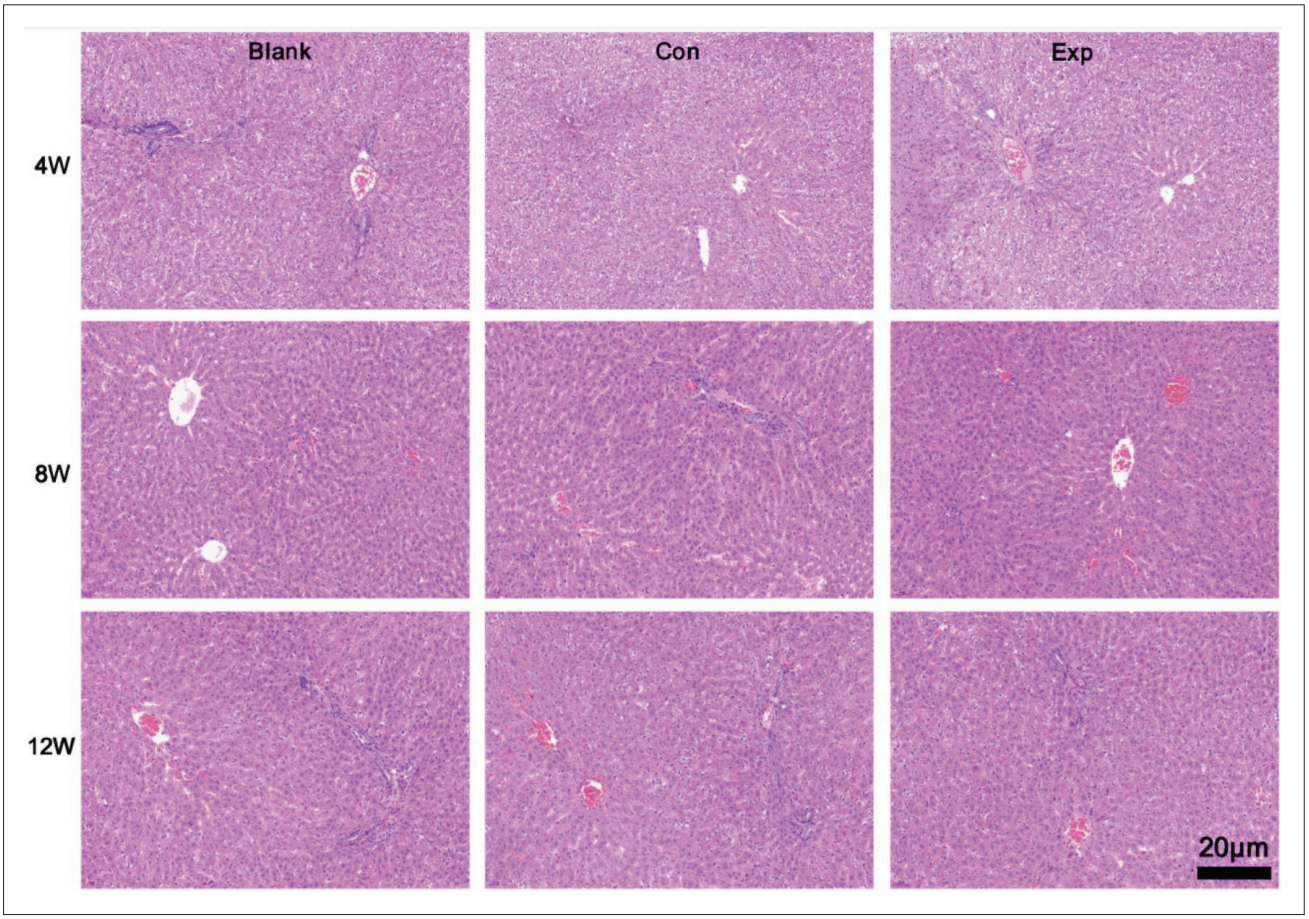

Figure 11. Hematoxylin and eosin staining of rat livers in each group at 4, 8, and 12 weeks postoperatively. Scale bar: 20 μm. Magnification: 40×. Notes: Blank: no scaffold; Control: treated with the PCL scaffold; Exp: treated with the PDA-PCL scaffold.

strength of human cortical bone ranges from 100 to 230 MPa and cancellous bone ranges from 2 to 12 MPa, the experimental results showed that the compressive strength of the PDA-PCL scaffolds was approximately 8 MPa. This value is sufficient for repairing bone defects in non-load-bearing areas.[34]

Before clinical application, tissue-engineered artificial bones must undergo biosafety testing, primarily focusing on the biocompatibility and cytotoxicity of the scaffolds.[35] To evaluate the biocompatibility of PDA–PCL composite scaffolds, BMSCs were seeded on PCL, PDA-PCL-3, PDA-PCL-6, and PDA-PCL-24 scaffolds. The results (Figure 3) showed that cell proliferation rates on modified scaffolds were higher than on plain PCL scaffolds, suggesting that PDA modification enhanced cell adhesion and proliferation. Importantly, PDA-coated PCL scaffolds did not exhibit cytotoxicity. Among the groups, scaffolds modified for 6 h (PDA-PCL-6) demonstrated the strongest ability to promote cell proliferation, with statistically significant differences.

Alkaline phosphatase is an early marker of osteoblast differentiation, and its activity is closely related to osteogenic potential, providing a preliminary assessment of the osteogenic performance of implanted materials.[36] Calcium nodule deposition, one of the hallmarks of advanced osteoblast maturation, further reflects the osteogenic capacity of scaffolds. In this study, PDA coating was shown to enhance the biological activity of PCL scaffolds, as demonstrated by ALP staining, alizarin red staining, and quantitative detection of calcium nodule deposition (Figure 4).

In terms of osteogenic gene expression, *Runx2*, a transcription factor in the bone morphogenetic protein (BMP) signaling pathway, is a major regulator of osteoblast development and bone formation. It is considered one of the earliest transcription factors to trigger osteogenic differentiation. ALP, widely recognized as a marker of osteoblast activity, represents an early phenotypic indicator of osteoblast and osteoclast differentiation. Additionally, COL-I is essential for bone tissue mineralization,

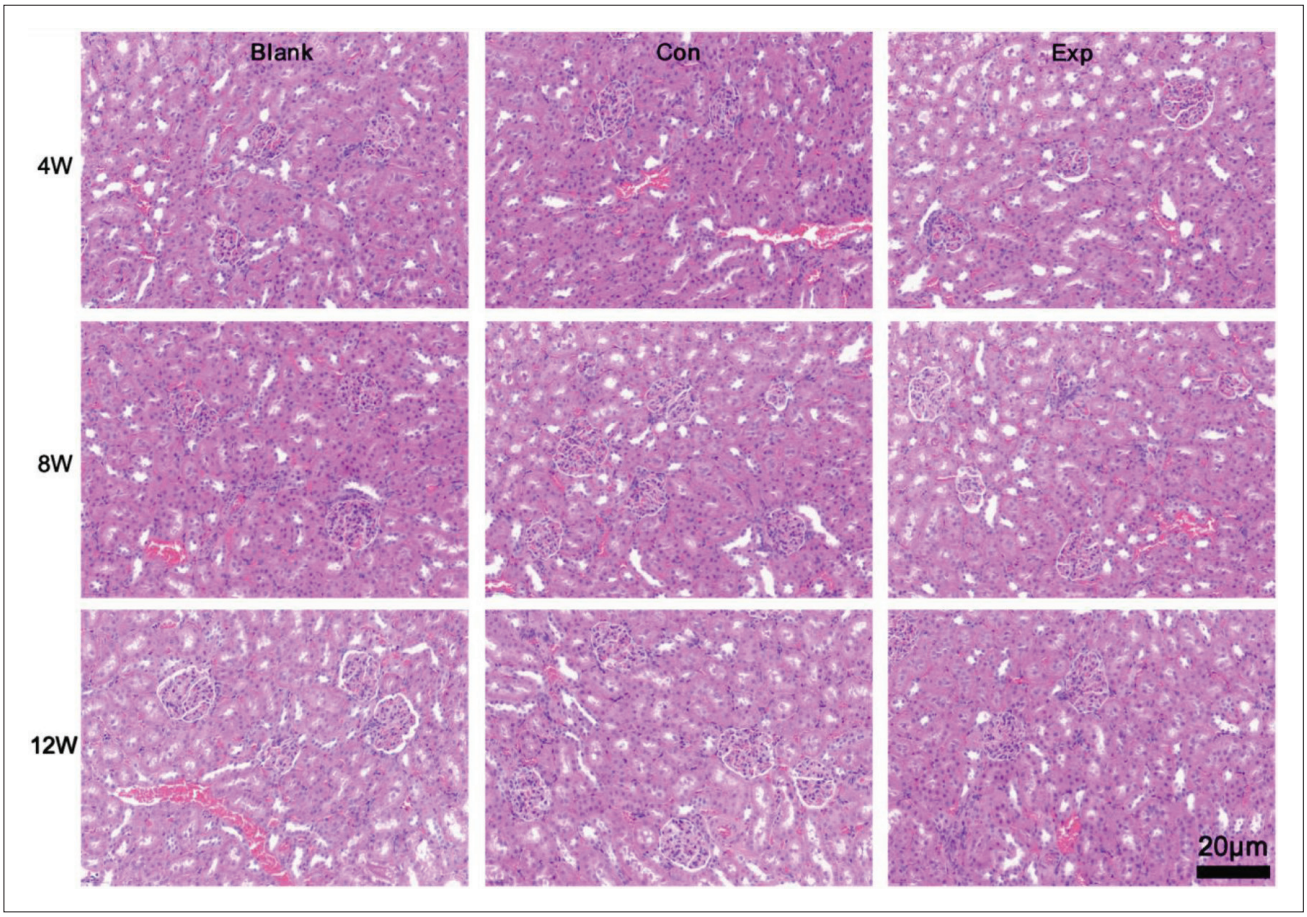

Figure 12. Hematoxylin and eosin staining of rat kidneys in each group at 4, 8, and 12 weeks postoperatively. Scale bar: 20 μm. Magnification: 40×. Notes: Blank: no scaffold; Control: treated with the PCL scaffold; Exp: treated with the PDA-PCL scaffold.

stimulating osteoblast adhesion and differentiation, and contributing to the formation of the organic matrix and structural integrity of cells.

In this study, the expression levels of *Runx2*, *Alp*, and *Col1* were measured using RT-PCR. Among the tested groups, the PDA-PCL-6 scaffolds exhibited the highest expression of these genes, followed by PDA-PCL-3. *Alp* expression levels in the PCL group were higher than in the PDA-PCL-24 group. No significant differences in *Col1* expression were observed between the PDA-PCL-0 and PDA-PCL-24 groups. These findings indicate that the PDA-PCL-6 group demonstrated the most significant osteogenic activity among the four groups.

Polydopamine degrades into a water-soluble compound in strongly alkaline solutions but remains essentially nondegradable in acidic and neutral environments, maintaining the original structure of DA during *in vitro* experiments.[37] DA activates DA receptors and induces ERK phosphorylation, thereby promoting osteogenic differentiation in BMSCs.[38,39] The appropriate PDA coating thickness plays a critical role in achieving superior cell adhesion and bone-enhancing properties, as excessively high DA concentrations may inhibit BMSC growth.

Sun et al.[40] demonstrated that a gradual increase in DA concentration (0.5–10 nM) favored osteogenic differentiation, while the DA-stimulated osteogenic performance diminished gradually at concentrations above 10 nM. Nonetheless, DA-mediated bone activity at 50 nM remained significantly higher than that at 5 nM. In this study, the DA concentration released by PDA-PCL-6 scaffolds ranged from 33–44 nM (Figure 2E), demonstrating exceptional osteoinductive performance. In addition, Pei et al.[41] found that DA concentrations below 2 mg/mL promoted macrophage polarization toward the M2 phenotype and reduced the secretion of inflammatory factors. All three groups of PDA-coated scaffolds in this study released DA below 2 mg/mL, confirming their excellent immunomodulatory properties. Unexpectedly, DA concentrations of 33–44 nM further enhanced macrophage polarization toward the M2 phenotype.

To evaluate the healing effects of PDA-coated scaffolds on cranial defects in rats, micro-CT imaging was performed on the cranial defect sites in each group. The new bone volume fraction was quantitatively analyzed and found to follow the trend: PDA-PCL group > PCL group > control group, with statistically significant differences between groups (Figure 5). Histological staining further corroborated these findings, revealing a progressive increase in new bone formation in the bone defect area of the PDA-PCL group over time. By week 12, as the implanted scaffold gradually degraded, the bone defect area in the experimental group (PDA-PCL group) was nearly filled with new bone tissue, followed by the control group (PCL group), while the blank group exhibited the least amount of new bone (Figures 6–8).

Immunohistochemical staining was utilized to further evaluate the repair of cranial bone defects in rats. The expressions of BMP-2 and COL-I, critical growth factors for bone tissue development, were analyzed. These factors play pivotal roles during new bone formation by inducing the differentiation of osteoblasts into osteogenic cells and promoting the reverse differentiation of fibroblasts, myoblasts, and bone marrow precursor cells into osteogenic cells.[42,43]

Immunohistochemical staining was performed on rat calvarial specimens from each group at 4, 8, and 12 weeks postoperatively. Results demonstrated that the expression of osteogenesis-related proteins in the PDA-PCL group was significantly higher than that in the blank and PCL groups across all time points. Additionally, blood indices and H&E-stained sections of the liver and kidney from rats in all groups showed no evident abnormalities, indicating that the PDA-functionalized PCL scaffolds exhibited excellent *in vivo* biocompatibility. These findings suggest that the PDA-functionalized coating significantly enhanced cell adhesion and conferred osteoinductive properties to the PCL scaffolds. In addition, the PDA–PCL composite scaffolds effectively promoted the repair of cranial bone defects in rats. However, this study only preliminarily investigated their effects on small cranial bone defects in rats. The potential of PDA-PCL scaffolds to repair segmental bone defects in other anatomical locations or larger volumes requires further in-depth studies.

5. Conclusion

This study successfully developed 3D-printed PCL composite scaffolds with a highly bioactive PDA coating. Compared with pure PCL scaffolds, the PDA-coated scaffolds, especially those in the PDA-PCL-6 group, demonstrated immunomodulatory properties and significantly enhanced the proliferation and adhesion of BMSCs as well as osteogenic differentiation. In addition, the PDA-coated scaffolds effectively facilitated the repair of cranial bone defects in rats while exhibiting excellent histocompatibility, offering a promising new approach to the treatment of bone defects. Nonetheless, further studies are necessary to evaluate the efficacy of these scaffolds in repairing larger or more extensive bone defects.

Acknowledgments

None.

Funding

This research was supported by the National Natural Science Foundation of China (32000964, 82160577), the Guangdong Province Science and Technology Plan Project (2024A1515012265, 2020B1111560001, and 2022A1515140193), the Program for Science and Technology Project of Guizhou Province, Qiankehe Platform Talents ([2021] 5613), the Key Program for Science and Technology Project of Guizhou Province (ZK [2021] 007), the GDAS' Project of Science and Technology Development (2022GDASZH-2022020402-01, 2022GDASZH-2022010110, 2020GDASZH-2022030604-01, and 2023GDASZH-2023010102).

Conflict of interest

We declare that we have no financial and personal relationships with other people or organizations that can inappropriately influence our work, and there is no professional or other personal interest of any nature or kind in any product, service and/or company that could be construed as influencing the position presented in, or the review of, the manuscript entitled.

Author contributions

Conceptualization: Qian Zhong, Shuai Huang, Weihua Huang, Weikang Xu, Qingde Wa

Data curation: Qian Zhong, Shuai Huang, Weihua Huang, Weikang Xu, Qingde Wa

Formal analysis: Qian Zhong, Shuai Huang, Weihua Huang

Funding acquisition: Weikang Xu, Qingde Wa

Investigation: Qian Zhong, Shuai Huang, Weihua Huang

Methodology: Qian Zhong, Shuai Huang, Weihua Huang

Project administration: Qian Zhong, Shuai Huang, Weihua Huang, Hengpeng Wu, Yang Wang, Zhenyu Wen, Huinan Yin, Yixiao Wang

Resources: Qian Zhong, Shuai Huang, Weihua Huang

Software: Qian Zhong, Shuai Huang, Weihua Huang

Validation: Weikang Xu, Qingde Wa
Visualization: Weikang Xu, Qingde Wa
Writing – original draft: Qian Zhong, Shuai Huang, Weihua Huang
Writing – review & editing: Weikang Xu, Qingde Wa

Ethics approval and consent to participate

All animal experiments were performed under the protocol approved by the Institutional Animal Care and Use Committee of Guangdong Quality Supervision and Testing Station for Medical and Health Care Appliances (Ethics approval number: 32000964).

Consent for publication

Not applicable.

Availability of data

Data are available from the corresponding author upon reasonable request.

References

1. Nauth A, McKee MD, Einhorn TA, Watson JT, Li R, Schemitsch EH. Managing bone defects. *J Orthop Trauma*. 2011;25(8):462-466.
doi: 10.1097/BOT.0b013e318224caf0

2. Schemitsch EH. Size matters: defining critical in bone defect size! *J Orthop Trauma*. 2017;31(Suppl 5):S20-S22.
doi: 10.1097/BOT.0000000000000978

3. Khodakaram-Tafti A, Mehrabani D, Shaterzadeh-Yazdi H, Zamiri B, Omidi M. Tissue engineering in maxillary bone defects. *World J Plast Surg*. 2018;7(1):3-11.

4. Dewey MJ, Milner DJ, Weisgerber D, et al. Repair of critical-size porcine craniofacial bone defects using a collagen-polycaprolactone composite biomaterial. *Biofabrication*. 2021;14(1):1-24.
doi: 10.1088/1758-5090/ac30d5

5. van der Heide D, Cidonio G, Stoddart MJ, D'Este M. 3D printing of inorganic-biopolymer composites for bone regeneration. *Biofabrication*. 2022;14(4):1-22.
doi: 10.1088/1758-5090/ac8cb2

6. Turnbull G, Clarke J, Picard F, et al. 3D bioactive composite scaffolds for bone tissue engineering. *Bioact Mater*. 2017;3(3):278-314.
doi: 10.1016/j.bioactmat.2017.10.001

7. Gharibshahian M, Salehi M, Beheshtizadeh N, et al. Recent advances on 3D-printed PCL-based composite scaffolds for bone tissue engineering. *Front Bioeng Biotechnol*. 2023;11:1168504.
doi: 10.3389/fbioe.2023.1168504

8. Nobles KP, Janorkar AV, Williamson RS. Surface modifications to enhance osseointegration-Resulting material properties and biological responses. *J Biomed Mater Res B Appl Biomater*. 2021;109(11):1909-1923.
doi: 10.1002/jbm.b.34835

9. Gharibshahian M, Salehi M, Kamalabadi-Farahani M, Alizadeh M. Magnesium-oxide-enhanced bone regeneration: 3D-printing of gelatin-coated composite scaffolds with sustained Rosuvastatin release. *Int J Biol Macromol*. 2024;266(Pt 1):130995.
doi: 10.1016/j.ijbiomac.2024.130995

10. Kikionis S, Ioannou E, Aggelidou E, et al. The marine polysaccharide ulvan confers potent osteoinductive capacity to PCL-based scaffolds for bone tissue engineering applications. *Int J Mol Sci*. 2021;22(6):3086.
doi: 10.3390/ijms22063086

11. Wang B, Zeng Y, Liu S, et al. ZIF-8 induced hydroxyapatite-like crystals enabled superior osteogenic ability of MEW printing PCL scaffolds. *J Nanobiotechnol*. 2023;21(1):264.
doi: 10.1186/s12951-023-02007-w

12. Ha YM, Kim YN, Jung YC. Rapid and local self-healing ability of polyurethane nanocomposites using photothermal polydopamine-coated graphene oxide triggered by near-infrared laser. *Polymers*. 2021;13(8):1274.
doi: 10.3390/polym13081274

13. Yan J, Wu R, Liao S, Jiang M, Qian Y. Applications of polydopamine-modified scaffolds in the peripheral nerve tissue engineering. *Front Bioeng Biotechnol*. 2020;8:590998.
doi: 10.3389/fbioe.2020.590998

14. Rezk AI, Ramachandra Kurup Sasikala A, Nejad AG, et al. Strategic design of a mussel-inspired in situ reduced Ag/Au-nanoparticle coated magnesium alloy for enhanced viability, antibacterial property and decelerated corrosion rates for degradable implant applications. *Sci Rep*. 2019;9(1):117.
doi: 10.1038/s41598-018-36545-3

15. Teixeira BN, Aprile P, Mendonça RH, Kelly DJ, Thiré RM da SM. Evaluation of bone marrow stem cell response to PLA scaffolds manufactured by 3D printing and coated with polydopamine and type I collagen. *J Biomed Mater Res B, Appl Biomater*. 2019;107(1):37-49.
doi: 10.1002/jbm.b.34093

16. Lin Y, Ou Y, Xu M, Chen J. Enhancing bone regeneration with bionic hydrolysis and biomimetic polydopamine coating on 3D-printed PCL scaffolds: a comparative study. *Mater Today Commun*. 2023;37:107262.
doi: 10.1016/j.mtcomm.2023.107262

17. Xu Z, Wang N, Liu P, et al. Poly(Dopamine) coating on 3D-printed poly-lactic-co-glycolic acid/β-tricalcium phosphate scaffolds for bone tissue engineering. *Molecules*. 2019;24(23):4397.
doi: 10.3390/molecules24234397

18. Lee H, Dellatore SM, Miller WM, Messersmith PB. Mussel-inspired surface chemistry for multifunctional coatings. *Science*. 2007;318(5849):426-430. doi: 10.1126/science.1147241

19. Li Y, Yang L, Hou Y, et al. Polydopamine-mediated graphene oxide and nanohydroxyapatite-incorporated conductive scaffold with an immunomodulatory ability accelerates periodontal bone regeneration in diabetes. *Bioact Mater*. 2022;18:213-227. doi: 10.1016/j.bioactmat.2022.03.021

20. Zhou S, Liu S, Wang Y, et al. Advances in the study of bionic mineralized collagen, PLGA, magnesium ionomer materials, and their composite scaffolds for bone defect treatment. *J Funct Biomater*. 2023;14(8):406. doi: 10.3390/jfb14080406

21. Guo R, Zhang R, Liu S, et al. Biomimetic, biodegradable and osteoinductive treated dentin matrix/α-calcium sulphate hemihydrate composite material for bone tissue engineering. *Regener Biomater*. 2023;10:rbad061. doi: 10.1093/rb/rbad061

22. Wang S, Gu R, Wang F, et al. 3D-Printed PCL/Zn scaffolds for bone regeneration with a dose-dependent effect on osteogenesis and osteoclastogenesis. *Mater Today Bio*. 2022;13:100202. doi: 10.1016/j.mtbio.2021.100202

23. Tang A, Ji J, Li J, et al. Nanocellulose/PEGDA aerogels with tunable poisson's ratio fabricated by stereolithography for mouse bone marrow mesenchymal stem cell culture. *Nanomaterials (Basel)*. 2021;11(3):603. doi: 10.3390/nano11030603

24. Wu Y, Liu J, Kang L, et al. An overview of 3D printed metal implants in orthopedic applications: present and future perspectives. *Heliyon*. 2023;9(7):e17718. doi: 10.1016/j.heliyon.2023.e17718

25. Dong J, Ding H, Wang Q, Wang L. A 3D-printed scaffold for repairing bone defects. *Polymers*. 2024;16(5):706. doi: 10.3390/polym16050706

26. Zhao Q, Gao S. Poly (butylene succinate)/silicon nitride nanocomposite with optimized physicochemical properties, biocompatibility, degradability, and osteogenesis for cranial bone repair. *J Funct Biomater*. 2022;13(4):231. doi: 10.3390/jfb13040231

27. Jia L, Han F, Wang H, et al. Polydopamine-assisted surface modification for orthopaedic implants. *J Orthop Transl*. 2019;17:82-95. doi: 10.1016/j.jot.2019.04.001

28. Xiao L, Li Y, Geng R, et al. Polymer composite microspheres loading 177Lu radionuclide for interventional radioembolization therapy and real-time SPECT imaging of hepatic cancer. *Biomater Res*. 2023;27(1):110. doi: 10.1186/s40824-023-00455-x

29. Mahnavi A, Shahriari-Khalaji M, Hosseinpour B, et al. Evaluation of cell adhesion and osteoconductivity in bone substitutes modified by polydopamine. *Front Bioeng Biotechnol*. 2022;10:1057699. doi: 10.3389/fbioe.2022.1057699

30. Du J, Zhou Y, Bao X, et al. Surface polydopamine modification of bone defect repair materials: Characteristics and applications. *Front Bioeng Biotechnol*. 2022; 10:974533. doi: 10.3389/fbioe.2022.974533

31. Caihong T, Fusheng M, Baoyong L, et al. Research status of the surface modification method based on polydopamine [in Chinese]. Chem Bull 2015;78: 983-990. doi: 10.14159/j.cnki.0441-3776.2015.11.003

32. Huang S, Liang N, Hu Y, Zhou X, Abidi N. Polydopamine-assisted surface modification for bone biosubstitutes. *BioMed Res Int*. 2016;2016:2389895. doi: 10.1155/2016/2389895

33. Li H, Zhao T, Cao F, et al. Integrated bioactive scaffold with aptamer-targeted stem cell recruitment and growth factor-induced pro-differentiation effects for anisotropic meniscal regeneration. *Bioeng Transl Med*. 2022; "7(3):e10302. doi: 10.1002/btm2.10302

34. Chang B, Liu X. Osteon: Structure, Turnover, and Regeneration. *Tissue Eng Part B Rev*. 2022;28(2):261-278. doi: 10.1089/ten.TEB.2020.0322

35. V K AD, Ray S, Arora U, Mitra S, Sionkowska A, Jaiswal AK. Dual drug delivery platforms for bone tissue engineering. *Front Bioeng Biotechnol*. 2022;10:969843. doi: 10.3389/fbioe.2022.969843

36. Ma YX, Jiao K, Wan QQ, et al. Silicified collagen scaffold induces semaphorin 3A secretion by sensory nerves to improve in-situ bone regeneration. *Bioact Mater*. 2022;9:475-490. doi: 10.1016/j.bioactmat.2021.07.016

37. Chen X, Yang W, Zhang J, Zhang L, Shen H, Shi D. Alkalinity triggered the degradation of polydopamine nanoparticles. *Polym Bull*. 2021;78(8):4439-4452. doi: 10.1007/s00289-020-03312-2

38. Wang CX, Ge XY, Wang MY, Ma T, Zhang Y, Lin Y. Dopamine D1 receptor-mediated activation of the ERK signaling pathway is involved in the osteogenic differentiation of bone mesenchymal stem cells. *Stem Cell Res Ther*. 2020;11(1):12. doi: 10.1186/s13287-019-1529-x

39. Xia S, Liu D, Jiang K, et al. Photothermal driven BMSCs osteogenesis and M2 macrophage polarization on polydopamine-coated Ti3C2 nanosheets/poly(vinylidene fluoride trifluoroethylene) nanocomposite coatings. *Mater Today Bio*. 2024;27:101156.

doi: 10.1016/j.mtbio.2024.101156

40. Sun H, Feng Y, Tu S, et al. Dopamine promotes osteogenic differentiation of PDLSCs by activating DRD1 and DRD2 during orthodontic tooth movement via ERK1/2 signaling pathway. *Regen Ther*. 2024;27:268-278. doi: 10.1016/j.reth.2024.03.025

41. Pei D, Zeng Z, Geng Z, et al. Modulation of macrophage polarization by secondary cross-linked hyaluronan-dopamine hydrogels. *Int J Biol Macromol*. 2024;270:132417. doi: 10.1016/j.ijbiomac.2024.132417

42. Donkiewicz P, Benz K, Kloss-Brandstätter A, Jackowski J. Survival rates of dental implants in autogenous and allogeneic bone blocks: a systematic review. *Medicina (Kaunas)*. 2021;57(12):1388. doi: 10.3390/medicina57121388

43. Li X, Zhou Q, Wu Y, et al. Enhanced bone regenerative properties of calcium phosphate ceramic granules in rabbit posterolateral spinal fusion through a reduction of grain size. *Bioact Mater*. 2022;11:90-106. doi: 10.1016/j.bioactmat.2021.10.006